JOURNAL OF APPLIED ELECTROCHEMISTRY **27** (1997) 762–773

Smooth Raney nickel coatings for cathodic hydrogen evolution by chemical gas phase reaction of nickel electrode surfaces

Th. BORUCINSKY, S. RAUSCH, H. WENDT

Institut für Chemische Technologie, TH Darmstadt, Petersenstrasse 20, D - 64287, Darmstadt, Germany

Received 26 March 1996; revised 14 August 1996

Two different processes to prepare smooth* Raney nickel coatings are investigated. Both are based on preparing a precursor coating by gas-phase reaction of nickel at temperatures of around 400 °C. Sherardizing of nickel electrodes, that is, reaction with zinc vapour, leads to formation of the γ-phase of Ni–Zn alloy with the approximate composition of 75 to 85 wt % Zn (balance: Ni), and gas-phase sulfidizing of nickel electrodes with hydrogen sulfide produces nickel sulfide coatings composed of the phases Ni_3S_2, αNi_7S_6 and αNiS. Both types of coating are transformed *in situ*, the first by caustic leaching and the second during cathodic hydrogen evolution by relatively slow cathodic reduction into smooth, almost closed nanoporous Raney nickel coatings. The comparison of the catalysts from the two different methods reveals the superiority of the second. The hydrogen evolution overpotential is lowest and, during more than 3000 h of continuous operation, the catalyst does not deteriorate. Electrodeposited nickel sulfide gives a poorer and less stable RN catalyst than gas phase sulfidized nickel sulfide.

1. Introduction

Cheap and reliable electrocatalytic activation of hydrogen evolving cathodes, in particular for alkaline electrolytes like caustic potash or sodium hydroxide, has been a long lasting issue for the electrochemical engineer dealing with the chloralkali process and alkaline water electrolysis. Numerous reviews on hydrogen electrocatalysts and catalysis have been published, the most recent being that of Trasatti [1]. Two principally different modes of catalytic activation of nickel supports are currently applied: the use of coatings of RuO_2 or modified RuO_2 and Raney nickel (RN).

The use of RuO_2 is not yet a well established technology and is also relatively expensive whereas the preparation of RN coatings has been performed commercially for more than thirty years [2, 3]. The different ways of applying precursor coatings from which RN can be prepared, for instance by caustic *in situ* leaching of Ni/Al or Ni/Zn precursors, have been described elsewhere [4–15]. There exist two different types of RN coatings, namely, composite coatings and smooth coatings. Composite coatings have a dual porosity, namely micro- and nanoporosity† and are composed of 5 to 10 μm granules of RN produced by slurry deposition, cold rolling or plasma spraying of nanoporous precursor alloy particles on a nickel support. Smooth, more or less closed, RN coatings (usually of 50 to 200 μm thickness) are obtained by preparing coherent and closed precursor alloy coatings on massive nickel supports, for instance by cathodically codepositing nickel and zinc.

Composite, as well as smooth, coatings exhibit very flat overpotential against log current density curves with low overpotentials, in particular in the current density range up to 0.4 A cm^{-2}. At temperatures ranging from 80 to 120 °C (in 40 wt % caustic potash) their potential against log i correlations exhibit slopes of less than -100 mV decade^{-1}. However, it is often observed with composite RN coatings that the slope of the current potential curve increases at higher current densities equalling or even exceeding -120 mV or more precisely 2.302 ($RT/\alpha F$) per dec. at 1 A cm^{-2} (compare for instance the most recent data of Lasia and coworkers [5–10] and of the present authors [16]).

In contrast, the semilogarithmic current potential curves of smooth coatings, which are nanoporous and homogeneous, are linear with low slopes of between -40 and -70 mV decade^{-1} over at least two

* Smooth RN coatings, in contrast to composite RN coatings, which usually have a more or less well defined microporosity in addition to the nanoporosity of the catalyst particles proper, form an essentially coherent nanoporous layer on the support. Although smooth coatings might be occasionally divided by cracks, the greater part of the catalyst is not subdivided and therefore these cracks are insignificant with respect to the effective catalytic activity of the coating.

† The present authors apply the terms 'micropore' and 'microporous' to porous materials whose pores range from 0.1 to 100 μm and they speak of 'nanoporosity' if pores from 1 to 100 nm are adressed.

0021-891X

Table 1. Gibbs energy and equilibrium ratio $p(H_2)/p(H_2S)$ for the reaction $Ni + H_2S \rightleftharpoons NiS + H_2$, [24]

	300 K	*700 K*
$\Delta G°$(NiS)/kJ mol	−56.970	−23.027
$\{p(H_2)/p(H_2S)\}$ equil.	5.83×10^9	52.3

orders of magnitude of current density up to current densities exceeding $1\,A\,cm^{-2}$. They are, therefore, superior to composite coatings as they yield low overpotentials at high current densities [17]. It is the aim of this work to investigate and characterize reliable methods for the preparation of smooth Raney nickel coatings. It has been demonstrated elsewhere that cathodically deposited Ni/Zn alloy precursor coatings were laminated and produced RN coatings of poorly reproducible catalytic activity. Lamination of low and high zinc layers caused blockage of highly active nanoporous RN by almost compact nickel layers [16]. Precursor coatings produced by gas phase reaction are expected to be more homogeneous and not irregularly stratified and their electrocatalytic activity should be more reproducible. Two different methods which use gas phase reactions for the production of smooth precursor layers on smooth nickel supports are compared to determine the electrocatalytic activity and the long-term behaviour of the RN coatings obtained therefrom over a time of at least 3000 h. The two methods are: (i) the formation of nickel/zinc precursor alloy coatings by sherardizing[‡] of nickel electrodes, and (ii) the formation of nickel sulfide coatings by gas phase sulfidizing nickel electrodes with hydrogen sulfide. Smooth RN coatings are subsequently generated by (i) caustic leaching and (ii) *in situ* cathodic reduction. The frequently reported catalytic activation of hydrogen cathodes by cathodic deposition of a mixture of X-ray amorphous nickel and nickel sulfide from electrolytes containing Ni^{2+} and thiosulfate has been included in this investigation. In addition, the Ni/S-phases Ni_3S_2, α-Ni_7S_6, α-$Ni_{1-x}S$, Ni_3S_4 and NiS_2 have been synthesized and cathodic hydrogen evolving electrodes formed from these compounds have been investigated.

2. Thermodynamic considerations concerning RN precursors

2.1. *Nickel zinc alloys*

The binary phase diagram of nickel and zinc is well established [18] and reproduced in [4]. Three high zinc Ni/Zn phases are documented with increasing zinc content [19]: the β_1-phase, stable below 675 °C with 50 ± 3 mol % Zn, the γ-phase, stable below 900 °C with 80 ± 4 mol % zinc, and the δ-phase stable below 480 °C with 88 ± 0.5 mol % zinc. At the upper Zn-concentration limit of the γ-phase the zinc activity coefficient amounts to approx. 0.05 at 300 °C [20, 21]. A partial excess heat of alloy formation of Zn of $-(23 \pm 2)\,kJ\,mol^{-1}$ [21] is obtained. Zinc in the β-, and even more in the γ- and δ-phase, can be easily dissolved and leached out of the alloy by 1 M or more concentrated aqueous caustic potash solution. From known stability coefficients of the zinc tetrahydroxo complex $[Zn(OH)_4]^{2-}$ [22], and the Gibbs energy of the corrosion reaction of Zn ($Zn + H_2O \rightarrow ZnO + H_2$) the standard Gibbs energy of the reaction

$$Zn(Ni, \gamma \text{ or } \delta) + 2H_2O + 2OH^- \rightarrow [Zn(OH)_4]^{2-} + H_2 \quad (1)$$

can be estimated to be of the order of $-100\,kJ\,mol^{-1}$. Therefore the precursor γ and δ NiZn phases deposited on nickel electrodes are readily decomposed in alkaline solution leaving behind a surface rich RN coating. At room temperature, leaching of a 50 μm layer of γ NiZn phase is almost complete within three hours.

2.2. *Nickel sulfides*

2.2.1. Formation of nickel sulfides. The binary phase diagram nickel/sulfur is well documented [18]. Phases which are stable at room temperature are (with increasing sulfur contents): Ni_3S_2, α-Ni_7S_6, α-$Ni_{1-x}S$, Ni_3S_4 and NiS_2. Generating these phases by reacting nickel with hydrogen sulfide at 0.1 MPa at temperatures of up to 400 °C should be possible for the three low sulfur phases up to NiS according to negative values of the standard Gibbs energy of the reaction shown in Equation 2.

$$Ni + xH_2S \rightleftharpoons NiS_x + xH_2 \quad (2)$$

As an example, the equilibrium ratios $p(H_2)/p(H_2S)$ and ΔG° for the phase NiS for 300 and 700 K are given in Table 1 [24].

It should also be possible to produce Ni_3S_4 and even NiS_2 at 700 K because at equilibrium a $p(H_2S)/p(H_2)$ ratio of approximately unity is calculated from the thermodynamic data for NiS_2 at 400 °C. Nickel sulfide layers produced by sulfidizing nickel electrodes with hydrogen sulfide do, however, contain neither Ni_3S_4 nor NiS_2 in measurable quantities. The reaction of nickel with sulfur does, however, lead to the formation of the higher nickel sulfides Ni_3S_4 and NiS_2.

2.2.2. Conversion of nickel sulfides to RN by cathodic reduction in alkaline electolytes. Using nickel sulfide coated nickel electrodes as hydrogen cathodes in caustic potash will lead to cathodic reduction of the nickel sulfide according to Equation 3, provided the corresponding equilibrium potential is equal to, or more positive than, the potential of the reversible hydrogen electrode in the respective electrolyte.

[‡] Sherardizing means annealing of nickel embedded in zinc powder (mean particle diameter 10 μm) at temperatures close to, but below the melting point of zinc (420 °C).

$$NiS_x + 2xe^- \rightarrow Ni + xS^{2-} \quad (3)$$

Calculating the Gibbs energy for Equation 3 and the equilibrium potential of this reaction with reference to the reversible hydrogen electrode (RHE) requires accounting for the Gibbs energy of Equation 2, and the pH or hydroxyl ion activity in the electrolyte as it determines the activity of hydrogen sulfide according to Equations 4 and 5.

$$H_2S + 2OH^- \rightleftharpoons 2H_2O + S^{2-} \quad (4)$$

$$a_{H_2S} = (K_{a1}K_{a2})^{-1} a_{s^{2-}} a_{OH^-}^{-2} K_{IP}^2 \quad (5)$$

Where K_{a1} and K_{a2} [22] are the first and second dissociation coefficients of hydrogen sulfide in water and K_{IP} is the ion product (10^{-14} M^2 at 20 °C) of water.

The thermodynamic calculation should also account for the production of RN. This means nickel with high specific surface. Assuming a typical value of 75 m^2 g^{-1} and a surface energy of 1 J m^{-2} [23] results in a Gibbs surface energy of approximately 4 kJ mol^{-1}. Figure. 1(a) and 1(b) depict the dependence of the equilibrium potential (298 K) of the cathodic desulfidizing reaction (Equation 3) against RHE on the sulfide anion concentrations in caustic electrolytes of $a_{OH^-} = 1$ M, (a), and for pH 15.7, which corresponds to 40 wt % KOH, (b) [25], at 298 K. The alkalinity and sulfide ion concentration are critical for the feasibility of the reaction for the lower sulfides. In an electrolyser sulfide ions would be oxidized anodically to polysulfide and eventually to sulfate and $a_{S^{2-}}$ may be assumed to stay below 10^{-3} M. At −30 mV vs RHE all nickel sulfide phases are unstable, not only in 40 wt % caustic potash, but even in 1 M NaOH or KOH solutions. Evolving cathodically hydrogen at nickel sulfide coated nickel electrodes would eventually lead to cathodic decomposition of the nickel sulfides to elemental nickel and sulfide anions. The extra cathodic overpotential neccessary to account for the generation of the inner surface of RN would be almost negligible and would not exceed −20 mV. Figure 1(a) and (b) hold for 298 K. At higher temperatures, for instance at the typical working temperature of 80 °C, the nickel sulfides become even more unstable.

3. Experimental details

3.1. *Formation of nickel sulfides and precursor coatings of NiS_x and Ni/Zn*

3.1.1. Synthesis of bulk nickel sulfide phases. For synthesis of nickel sulfur compounds nickel wire, 0.5 mm in diameter, (not the more reactive nickel powder), was used. This prevented too vigorous a

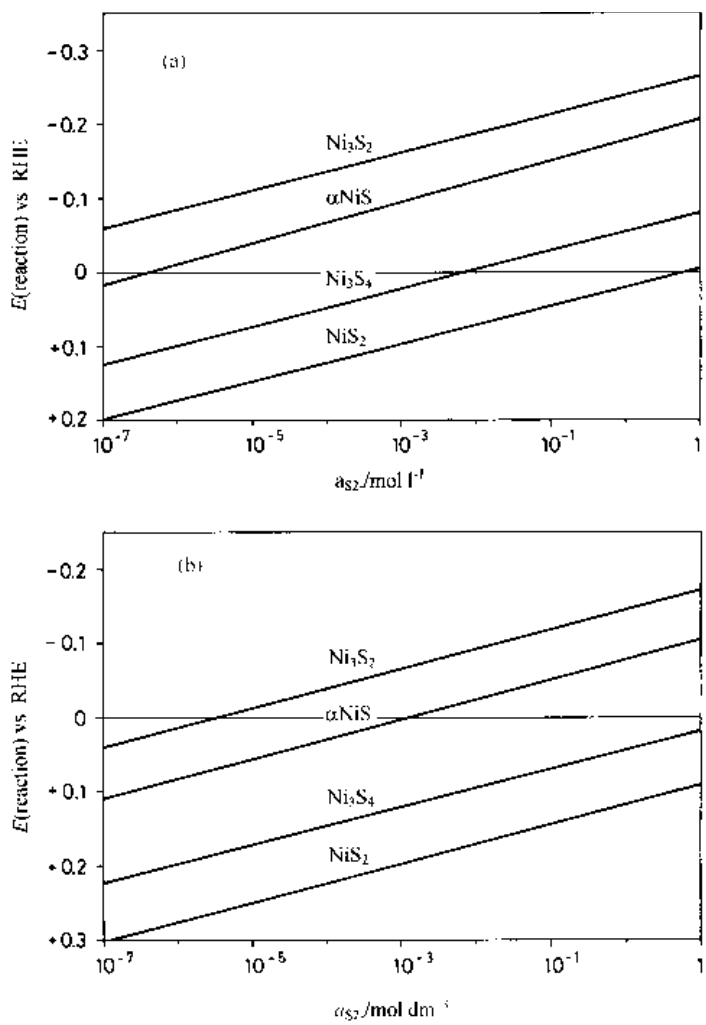

Fig. 1. Equilibrium potential of the reaction $NiS_x + 2xe^- \rightleftharpoons Ni + xS^{2-}$ calculated vs RHE in dependence on sulfide concentration in (a) 1 M KOH, pH 14 and (b) 40 wt % KOH, pH 15.7 at 25 °C.

reaction leading to overheating and explosion of the reaction vessel due to too high sulfur vapour pressures. The respective stoichiometric amount of sulfur was added to the wire and both were sealed under moderate vacuum (0.5 Pa) in a quartz ampoule. The specimens were heated within 48 h to 300 °C, and subsequently further above the melting point of the respective compound by stepping the temperature by 25 °C in 6 h intervals. Annealing for 120 h at 500, 390, 360, 340 and 280 °C for 3 h gave time for formation of the respective low temperature modifications of the different nickel sulfur phases. The higher sulfur phases Ni_3S_4 and NiS_2 are not molten, because at their melting points their sulfur vapour pressures surmount the safety limits and the ampoules explode. Therefore, Ni_3S_4 and NiS_2 electrodes were produced by isostatic pressing (1900 kN) the powder for 10 min followed by vacuum sintering at 780 °C for 100 h. According to X-ray diffraction in all cases the pure phases were formed, except for the preparation of Ni_3S_4. From the solidified compounds Ni_3S_2, Ni_7S_6 and NiS rectangular electrodes were produced by mechanical machining and grinding.

Electrical contacts to the sulfide electrodes were accomplished by etching one of the faces of the bulk nickel sulfide electrodes for 10 s with conc. H_3PO_4, rinsing with distilled water and soldering a nickel wire to this surface by tin solder. The nickel wire and the solder were protected against corrosion by Serifix Resin SQ. Polishing the active electrode surface with diamond paste removed any resin residues.

3.1.2. Sulfidizing smooth nickel supports by reaction with H_2S. Perforated nickel sheets supplied from Storck Co. with a hole diameter of 1.35 mm, 58% active nickel surface and 42% open area and a thickness of 250 μm, which were cut into coupons 2.5 cm × 2.5 cm, were connected to two 1 mm diameter nickel wires by point soldering. They were etched for 5 min in a solution composed of 5 ml 30 vol% H_2O_2 and 95 ml concentrated hydrochloric acid, rinsed with distilled water, wiped with a filter paper and weighed. They were subjected to gas phase sulfidizing with hydrogen sulfide in a closed quartz tube (50 cm × 50 mm) whose ground lid had three quickfit inlets: one for a thermocouple and two quartz tubes as inlet and outlet for the reacting gas. A tubular furnace whose temperature was regulated by a Eurotherm PID-controller allowed for a temperature difference of less than 2 °C along the reaction zone of 70 mm length. The growth rate of nickel sulfide layers was measured gravimetrically by interrupting the sulphidizing experiments at times by fast chilling under hydrogen sulfide. For phase analysis the sulfide coatings were detached from the substrate by scratching, ground and X-ray diffraction analysed.

3.1.3. Ni/Zn-coatings by sherardizing of nickel electrodes. Sherardizing is an old technology [26]. It consists of embedding steel or iron parts in zinc powder and heating them up to 300 °C. Formation of Zn alloys on the surface of the steel parts proceeds by reaction of iron with zinc vapours. This technical process was used to apply smooth Ni/Zn coatings on perforated nickel electrodes and nickel foils. The zinc powder was composed of granules measuring from 5 to 20 μm in diameter with an average of 8 μm. The kinetics of the formation of the coating were measured gravimetrically and by SEM after etching [27].

3.2. *Cathodic deposition of nickel sulfide*

According to [28] and [29] the following bath composition was chosen for cathodic deposition of nickel sulfide coatings:

$$0.1\ \text{M}\ Na_2S_2O_3,\ 0.06\ \text{M}\ NiCl_2,\ 0.16\ \text{M}\ H_3BO_3,\ 0.24\ \text{M}\ NiSO_4,\ \text{pH} \sim 6$$

The nickel sulfide coatings were deposited on perforated nickel sheets. During cathodic nickel sulfide deposition hydrogen evolution cannot be avoided because nickel sulfide is a good electrocatalyst for cathodic hydrogen evolution. Deposition took place in a thermostated beaker of 1.5 litre volume with vertically inserted electrode coupons 2.5 cm × 2.5 cm under conditions of natural convection. The rate of nickel sulfide deposition at temperatures from 20 to 80 °C and current densities from 5 to 80 mA cm^{-2} were investigated. Current efficiencies were not well defined because the composition of the deposit changed from Ni/S ≈ 1/1 to 3/1, mol/mol. The current yield increased with temperature from 70 to 94% (lower at lowest temperature and highest current density) but approached 95% at 80 °C. The surface of the coating was not smooth but was decorated with cauliflowerlike nobs or buds. As shown in Fig. 2 the coatings were brittle and tended to detach from the support on thermal cycling. The most active coatings, which had been used for this investigation, were obtained at 5 mA cm^{-2} and at 20 °C and proved to be relatively most stable on thermal cycling.

3.3. *Electrochemical measurements*

The perforated metal electrodes, prior to sherardizing, sulfidizing or cathodic coating were supplied with

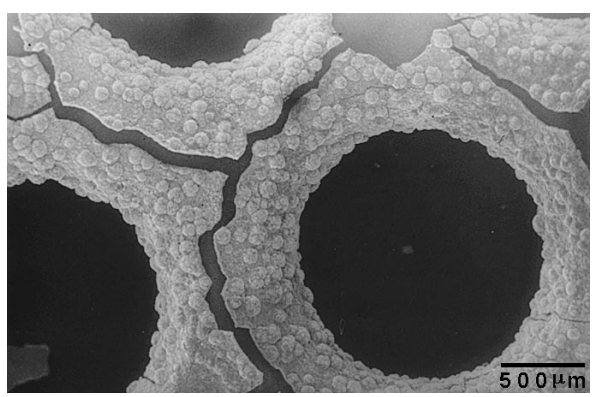

Fig. 2. Cathodically deposited nickel sulfide coating on perforated nickel foil after 3866 h of cathodic hydrogen evolution.

two point soldered nickel wires of 1 mm diameter. One carried the current, the second served as potential probe to eliminate in the switching experiments the ohmic potential drops of the lead, which is significant at $1\,A\,cm^{-2}$. The coating thickness of the nickel sulfide and the zinc–nickel alloy was 70 μm unless otherwise indicated. The zinc was leached for 3 h in cold, then in boiling 40 wt% KOH for 10 h. Subsequent boiling in distilled water for 2 h and exposing the moist electrode to air for 30 min stabilized the RN coating. During leaching the Ni/Zn coating shrank in thickness and laterally, forming cracks. The final smooth RN coating from Ni/Zn coatings of initially 75 μm thickness had a thickness of ~50 μm. Under cathodic hydrogen evolution nickel sulfide coatings lost almost all sulfur within several hundred hours, while they shrank in thickness by one third, but lateral shrinkage was not observed and cracks did not form. Electrolysis experiments were performed between room temperature and 120 °C in 40 wt% KOH solution. The electrolyte (350 cm^3) was pre-electrolysed using two smooth nickel electrodes to reduce iron traces in the electrolyte to less than 5 ppm. The electrolyte vessel was a PTFE-beaker equipped with a PTFE reflux condenser. The reference electrode was a reversible hydrogen electrode in the same electrolyte made of an immersed platinized platinum wire in contact with pure hydrogen. The Luggin capillary was a flexible PTFE tube of 1 mm diameter filled with pieces of polyphenylene sulfide cloth which prevented bubble formation and clogging of the PTFE tube. Current density potential correlations were measured from high to low current densities. IR corrections were performed by current interruption with a transistor switch developed at TH-Darmstadt ($\tau < 1\,\mu s$) and a storage oscilloscope (VUKO VKS 22–16).

3.4. *Determination of the inner surface of different RN coatings*

The coulometric determination of the inner surface of RN coatings is an established procedure, [17, 30, 31]. Its main principle is chronocoulometry using discontinuities of the electrode potential against time during galvanostatic oxidation of the catalyst to identify three different oxidation processes:

(i) the anodic oxidation of hydrogen, dissolved in the pore electrolyte or adsorbed on the inner surface,
(ii) the oxidation of the nickel surface atoms to a closed monolayer of nickel hydroxide $(NiOH)_2$, and
(iii) the further oxidation of $Ni(OH)_2$ to NiOOH.

A necessary precondition of this procedure is that the nickel particles in the catalysts are sufficiently large, so that a closed $Ni(OH)_2$ layer can be formed on them, preventing their further oxidation. As shown by Justi and coworkers, [30, 31], these particles measure at least 40 nm in diameter [32], so that the selective oxidation of surface nickel atoms at ambient temperature is assured. Further attack at defects or nanocracks might occur but seems to be of little significance. The nanoporous electrodes were galvanostatically oxidized at current densities of between 1.8 and $2.8\,mA\,cm^{-2}$ and the potential–time relation was recorded, evaluating the time of drastic potential change attributed to the oxidation of $Ni(OH)_2$ to NiOOH. Initially the electrodes evolved hydrogen for 12 h with an apparent current density of $400\,mA\,cm^{-2}$, 1 min at $2\,mA\,cm^{-2}$ and then an anodic current density of approximately $2\,mA\,cm^{-2}$ was applied.

4. Results

4.1. *Synthesis of NiS_x compounds*

The synthesis of different nickel sulfides lead, with one exception, to X-ray pure phases. Figure 3 shows the diffractogram of the low sulfur phase Ni_3S_2 and compares the diffractogram with reflexes obtained from [33]. An exception was the high sulfur phase Ni_3S_4. After annealing this specimen for 2100 h at 340 °C, besides Ni_3S_4, all other nickel sulfide phases which are stable at ambient temperature were detected.

4.2. *Growth and composition of precursor coatings by gas phase reactions*

4.2.1. Nickel sulfide coatings. Figure 4 shows the growth of nickel sulfide coatings on nickel in an atmosphere of 0.1 MPa H_2S as a plot of added mass per unit surface against the square root of t. From 300 ° to 450 °C the $\sqrt{t}$ law anticipated according to Tamm [34], and Pilling and Bedworth [35], is obeyed. That is,

$$\frac{dx}{dt} = k^* x^{-1} \tag{6a}$$

with x the coating thickness and k^* the rate of scale formation.

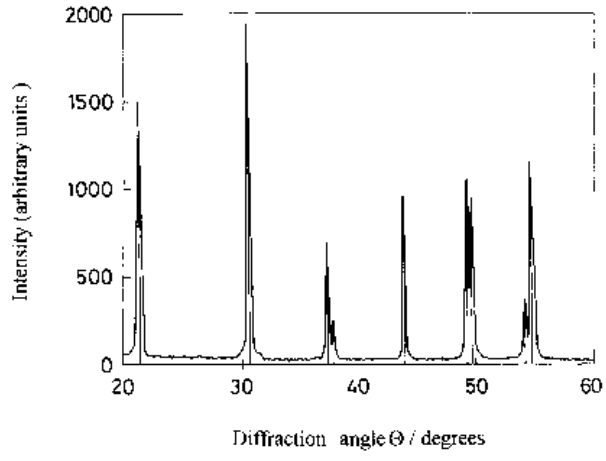

Fig. 3. X-ray diffractogram of synthesized bulk Ni_3S_2; lines reflect literature data [33].

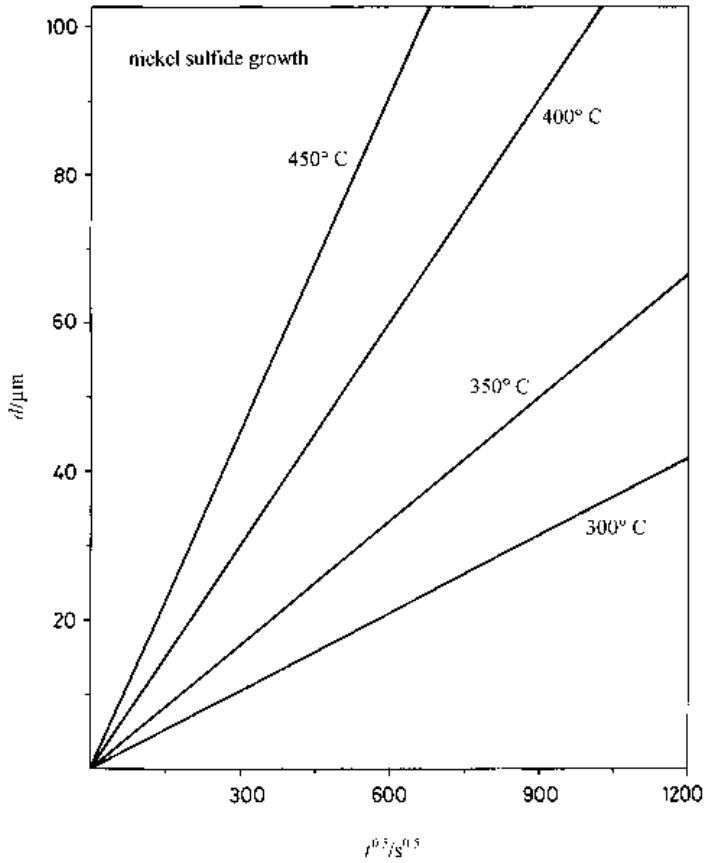

Fig. 4. Growth of nickel sulfide layers on nickel foil exposed to 0.1 MPa H_2S at different temperatures.

Since gravimetry is used to investigate coating growth Equation 5(a) is transformed into Equation 6(b). Thus,

$$\frac{dm}{dt} = km^{-1} \tag{6b}$$

with m the surface specific mass of coating and $k = k^* \rho^{-2} f_M$ with ρ the density of the coating and f_M the stoichiometric mass ratio explained below. The numerical equation of k for a broader range of temperature reads

$$k(NiS_x) = (0.27 \pm 0.2) \times 10^{-(3610 \pm 300)/T} / g^2 cm^{-4} s^{-1} \quad \text{(at 0.1 MPa } H_2S\text{)} \tag{6c}$$

This rate coefficient can be recalculated for k^* by using the relation $k^* = k\rho^{-2}[M(NiS)/M(S)]^2$ by assuming the nickel sulfide coatings to be in chemical composition and density very close to that of NiS. With $\rho(NiS) = 5.4\,g\,cm^{-3}$ the result is

$$k^*(NiS_{x\approx 1}) = (0.074 \pm 0.005) \times 10^{-(3610 \pm 300)/T} / cm^2 s^{-1} \tag{6d}$$

The growth is controlled by diffusive transport, very likely that of nickel ions, through the sulfide coating which is assumed to be layered. The activation energy of the transport process is $(62 \pm 6)\,kJ\,mol^{-1}$. We did not find data in the literature of sulfidizing rates of nickel by hydrogen sulfide but sulfidizing rates of iron in contact with liquid or gaseous sulfur are known. There also the square root law is observed [36–39].

The lowest layer of the NiS coating on nickel in contact with nickel metal is expected to be Ni_3S_2. Then there follow Ni_7S_6 and NiS and the uppermost layers are formed either by Ni_3S_4 and NiS_2 or only by Ni_3S_4. By X-ray analysis only Ni_3S_2, α-Ni_7S_6 and α-NiS were found with some additional diffraction lines which could not be attributed to any known Ni_xS_y compound, but certainly did not stem from NiS_2. In such sequences of layers the ratio of the thickness of the individual layers is given by the ratios of their respective growth rate or diffusivities of the relevant mobile species which is transported across the respective layer. Since, after short reaction times (2 h at 300 °C and 10 min at 450 °C), only Ni_3S_2 was detected in nickel sulfide coatings, this compound forms the fastest growing layer.

Figure 5a shows the surface of a sulfidized nickel foil, which had been exposed to 0.1 MPa H_2S at 400 °C for 142 min. A dense layer composed of coarse partially twinned nickel sulfide crystals were formed. Typically the electrodes possess a nickel core of 150 μm thickness and are covered from either side by a nickel sulfide coating of approximately 70 μm thickness. Because of the little optical contrast of nickel metal and the nickel sulfide coating in SEM micrographs polished cuts of these layers are not shown.

4.2.2. Nickel/zinc coatings by sherardizing nickel electrodes. The parabolic growth of nickel–zinc coatings in the sherardizing procedure was observed by gravimetry. The activation energy amounts to

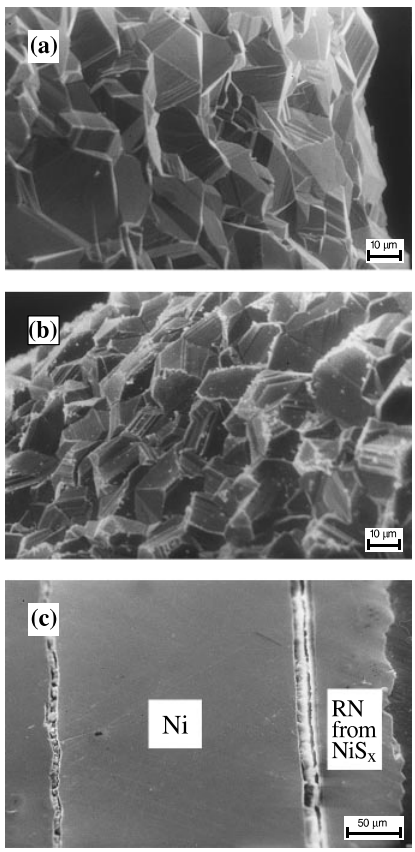

Fig. 5. Gas phase sulfidized nickel foil (thickness of NiS_x coating ≈ 75 μm). (a) surface of sulfide coating after formation, (b) surface of sulfide coating after cathodic hydrogen evolution for more than 3000 h, (c) cut through gas phase sulfidized nickel electrode after hydrogen evolution for more than 3000 h.

$(129 \pm 10)\,\mathrm{kJ\,mol^{-1}}$ and is almost double that of the growth for nickel sulfide layers. This value matches the heat of vaporization of solid zinc. The numerical equation of k for a broader range of temperature reads:

$$k(\mathrm{NiZn}) = (2.34 \pm 0.2) \times 10^{-(6190\pm400)/T}/\mathrm{cm^2 s^{-1}} \quad (7)$$

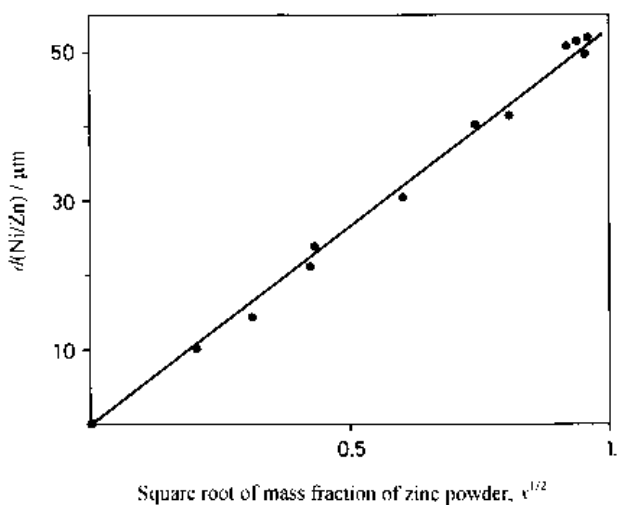

Fig. 6. Thickness of NiZn coating obtained by sherardizing nickel foils with sand added to zinc powder for 5 h at 390 °C in zinc/sand mixtures of different weight fractions, x, of zinc plotted against $\sqrt{x}$.

The rate coefficient diminishes as the zinc powder is diluted by addition of SiO_2 (sand) of appropriate granulometry (from 3 to 15 μm max.) as shown in Fig. 6. The thickness of the layer of Ni/Zn alloy grown at 300 °C during an experiment of 5 h duration increases with the square root of the mass fraction of the zinc dust in the zinc/silica mixtures. Obviously, mass transfer hindrance exists mainly on the side of the zinc granules, that is, on the gas side. Scanning electron micrographs show that the diffusive mass transport of zinc vapour through a layer of Zn-depleted ZnO vesicles, which initially coated the zinc granules, determines the growth rate of the alloy coating. Figure 8(a) shows a cut through such a dense and little structured Ni/Zn layer of ~150 μm thickness. This picture was selected because the cracks, which are usually very few, indicate some mechanical stress.

4.3. *Morphological and chemical changes during RN formation*

4.3.1. Nickel sulfide coatings. Figure 5 (b) shows the surface of nickel sulfide coatings after hydrogen evolution for more than 3000 h. A comparison with Fig. 5 (a) does not reveal significant differences (neglecting some deposits) and a cut through the coating (Fig. 5 (c)) shows an apparently homogeneous matrix with very few cracks, approximately one crack every 500 μm. (The catalyst layers in Fig. 5 (c) apparently

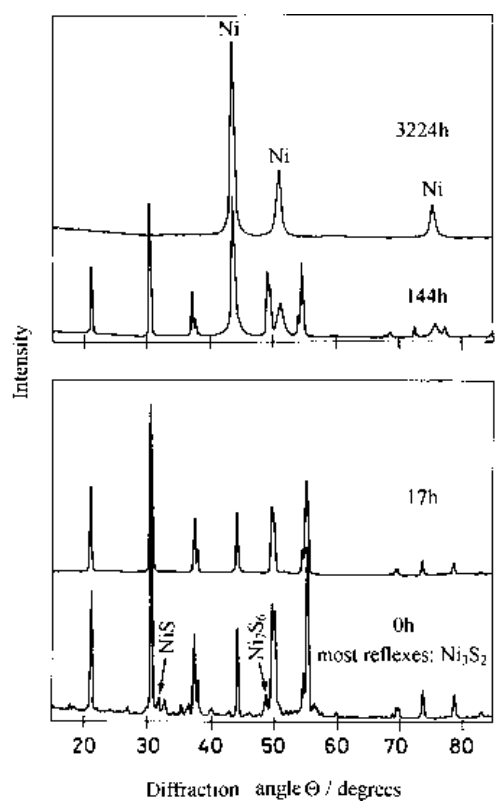

Fig. 7. X-ray diffraction pattern of NiS_x coatings from gas phase sulfidized nickel foils in dependence on exposure time to cathodic hydrogen evolution. Already after 144 h about 70% of the sulfide phases (mainly Ni_3S_2) has been converted to nanoporous Raney nickel.

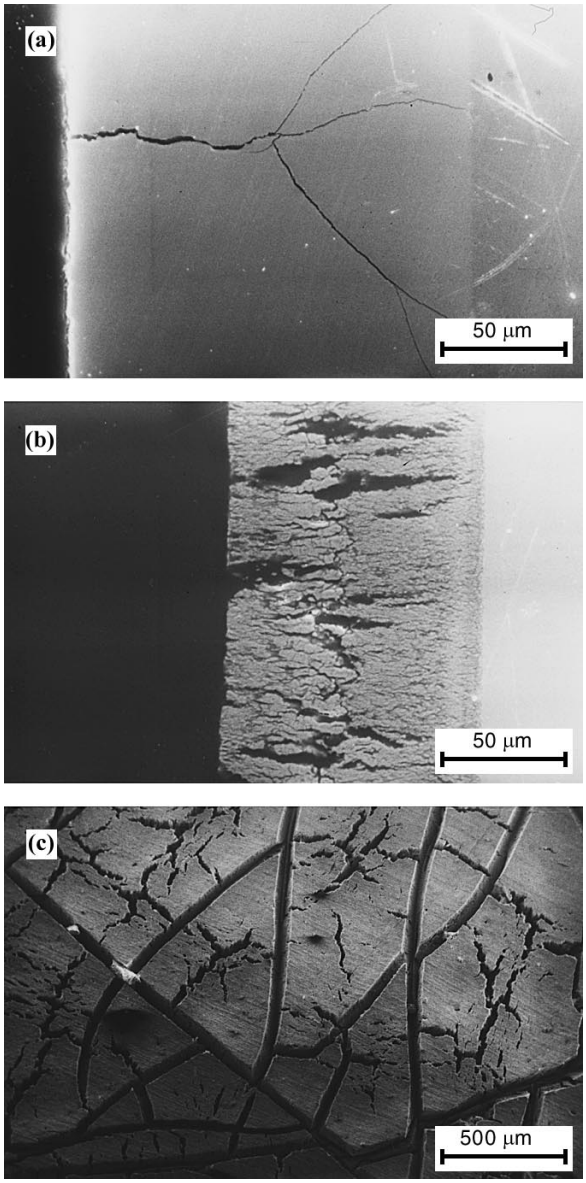

Fig. 8. Ni/Zn coatings. Cut of a coating: (a) as produced by sherardizing; (b) after alkaline leaching; (c) surface of coating after alkaline leaching.

have completely detached from the nickel support. This, however, is a secondary effect, which is caused by embedding the electrode into a polymer, which on hardening contracts exerting significant stress and strain on the embedded specimen.)

X-ray diffraction analysis of these catalyst layers shows that, after several hundred hours under cathodic load, they are no longer composed of nickel sulfide. After 144 h at least 50% of the phase Ni_3S_2 and all of Ni_7S_6 and NiS had disapperared and were converted to porous nickel (Fig. 7). After 3000 h all nickel sulfide had disappeared leaving behind an RN coating, whose coherent nanoparticles, according to the width of the X-ray reflexes, are 45 nm. Figure 7 (a) and (b) show the change of the X-ray diffraction pattern of such coatings during electrolytic hydrogen evolution. Chemical analysis of the highly porous RN coatings which, being more brittle than nickel can be peeled off, detects only 3% of the initially present sulfur after 3000 h. This also holds for cathodically deposited NiS_x coatings.

4.3.2. Zinc–nickel coatings. Figures 9 (b) and (c) show a cut through a nickel zinc coating and the surface of this coating after caustic leaching. The caustic dissolution of zinc leaves behind a RN coating which is not as homogeneous as the RN coatings from nickel sulfide. There exist coarser cracks whose width measure in micrometres and a fractal structure of submicrometre cracks, all more or less oriented perpendicular to the surface of the coating. The homogeneous slabs between the cracks are nanoporous and constitute the RN catalyst proper. This morphology does not change with time as these electrodes are used for hydrogen evolution, although after 3000 h the inner surface is diminished by approximately 50% due to slow recrystallization. The zinc content after leaching amounts to less than 1% of the initial zinc content and no zinc is left after 3000 h of hydrogen evolution. We cannot confirm the frequently published opinion that residual zinc is important for the catalytic activity of RN.

4.4. *Current potential curves*

4.4.1. Cathodes made of different bulk phase nickel sulfides. As the surface of nickel sulfide electrodes quickly loses sulfur in the form of sulfide anions in parallel to cathodic hydrogen evolution, current potential curves for cathodes made of the different sulfide phases were measured at 22 °C and after drawing a cathodic current of only 0.4 A cm^{-2} for no more than 10 min. Figure 9 compares the current potential curves measured on smooth nickel, on Ni_3S_2, α-Ni_7S_6 and NiS. Measurements on Ni_2S_3 and NiS_2 are not included because these compounds are chemically unstable, decomposing in contact with caustic potash. The Tafel plot at smooth nickel has a slope of −120 mV $decade^{-1}$ at ambient temperature, but at the different nickel sulfides slopes of less than –90 mV $decade^{-1}$ are observed. The difference between NiS and α-Ni_7S_6 is insignificant, both having a slope of −70 mV, whereas for Ni_2S_3 −80 mV $decade^{-1}$ are observed. These sulfides are excellent electrocatalysts for cathodic hydrogen evolution although they are not stable. The current voltage curves were reproduced several times within half an hour. Long performance tests were not performed.

4.4.2. Catalyst ageing at different RN electrodes

(a) *RN coatings from gas phase sulfidized nickel.* Figure 10 depicts the current potential curve for cathodic hydrogen evolution in 40 wt % caustic potash at 116 to 118 °C at gas phase sulfidized nickel electrodes with a sulfur loading of 45 mg S cm^{-2} which form RN coatings of roughly 50 μm thickness. The different current potential correlations in Fig. 10 were measured after cathodic hydrogen evolution at 1 A cm^{-2} for 21, 48, 1640 and 3224 h. After several 100 h the sulfur contents drops to almost zero. The

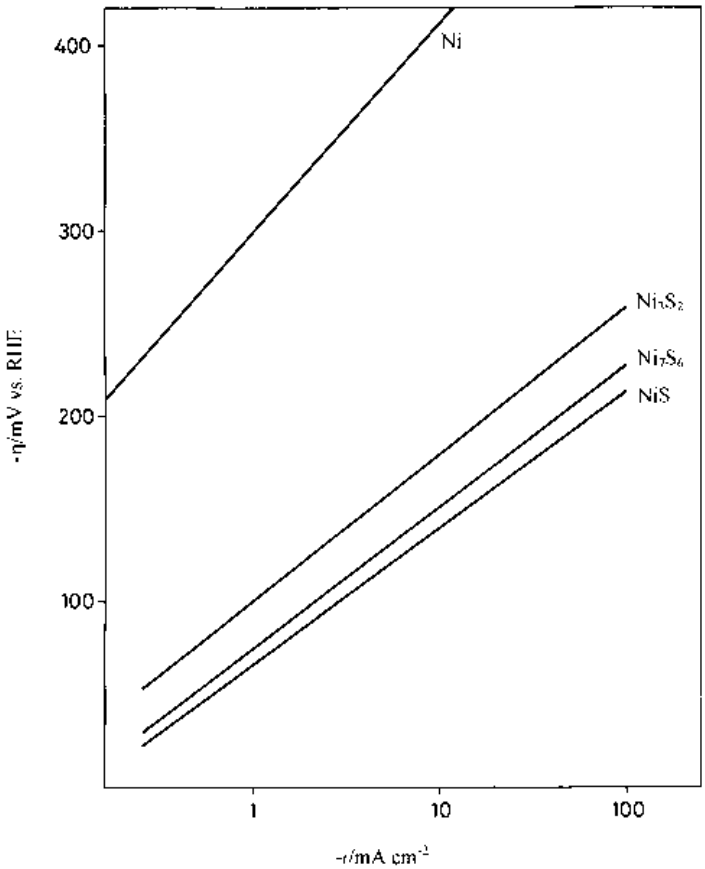

Fig. 9. $\log i$ against overpotential of cathodic hydrogen evolution at smooth nickel with electrodes made of different bulk nickel sulfides at 25 °C.

slope of the semilogarithmic current potential correlation does not vary with time and amounts approximately to only $-30\,\mathrm{mV\,decade^{-1}}$ extending from $10\,\mathrm{mA\,cm^{-2}}$ to $1\,\mathrm{A\,cm^{-2}}$. After 21 h the overpotential at $1\,\mathrm{A\,cm^{-2}}$ amounts to −95 mV and increases slowly by little more than −10 to −105 mV during continuous operation for more than 3000 h. This catalyst deteriorates only very slowly.

(b) *RN coatings from electrodeposited nickel sulfide.* In Fig. 10 the steeper current potential correlation with a slope of $-50\,\mathrm{mV\ decade^{-1}}$ measured at electrodeposited Ni_xS_y coatings also with a loading of $45\,\mathrm{mg\,S\,cm^{-2}}$ is recorded after 3000 h of hydrogen evolution at $1\,\mathrm{A\,cm^{-2}}$. The slope is steeper and at higher current densities the overpotential is higher than on gas phase sulfidized nickel with the same sulfur loading. It amounts to $-120\,\mathrm{mV}$ at $1\,\mathrm{A\,cm^{-2}}$.

(c) *RN coatings from sherardized nickel electrodes.* Figure 11 compares the current potential curves measured on RN coating (with a thickness of 50 μm) from sherardized nickel in 40 wt % caustic potash at 25 and 115 °C with measurements at smooth nickel electrodes (thin lines) [17]. The current potential curves, which are straight lines over several orders of magnitude of current density in the semilogarithmic plot are not extended below an overpotential of −20 mV in order to focus on the linear parts of the current potential curves. The slopes at RN are low measuring approximately −70 mV at ambient temperature and −80 mV per decade at 115 °C.

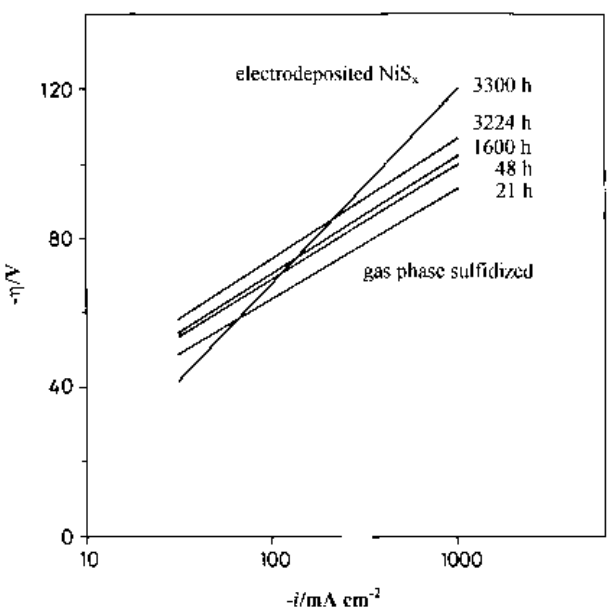

Fig. 10. Comparison of $\log i$ against overpotential correlations measured at gas phase sulfidized nickel electrodes after different times of cathodic hydrogen evolution and at cathodically deposited NiS_x coatings after 3000 h of operation. Electrolysis temperature in the range 116 to 118 °C.

4.5. *Dependence of overpotential on coating thickness*

4.5.1. RN coatings from gas phase sulfidized nickel. The thickness of RN coatings obtained from Ni_xS_y coatings was varied between 20 μm and 200 μm. A preelectrolysis of 200 h at $1\,\mathrm{A\,cm^{-2}}$ at 120 °C assured far reaching cathodic reduction of the coatings. For

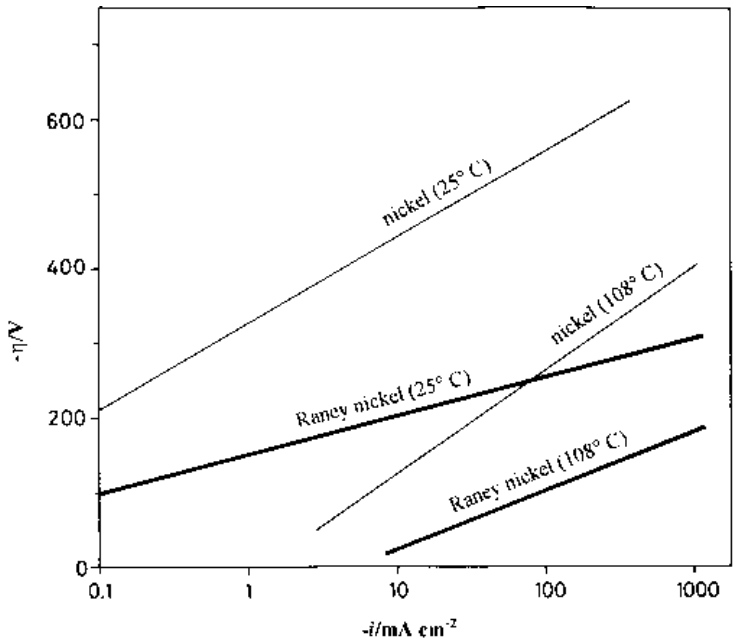

Fig. 11. $\log i$ against overpotential correlation of cathodic hydrogen evolution at smooth and sherardized nickel electrodes at 25 and 108 °C.

five different coatings thicknesses the current potential curves exhibited almost the same slope (50 ± 2 mV decade^{-1} at 120 °C). Figure 12 shows the dependence of overpotential on coating thickness in a semilogarithmic plot measured for six current densities from 50 to 1000 mA cm^2. For clarity only the lines obtained for 50 and 1000 mA cm^{-2} are shown, all other measurements lying between these limits in regular order. The correlation yields a slope of $d\eta/d \log d$ of 60 mV decade^{-1} for 50 mA cm^{-2} and 70 mV decade^{-1} for 1 A cm^{-2} at an electrolysis temperature of 120 °C. This dependence of overpotential on coating thickness is an obvious consequence of the coating porosity because with a compact coating only the surface would be electrocatalytically active with little influence of the coating thickness on the effective catalytic activity.

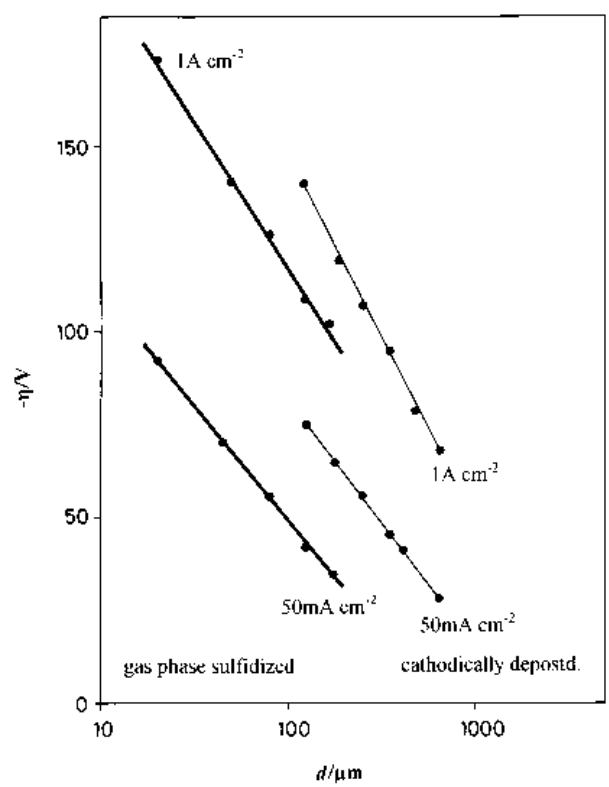

Fig. 12. Dependence of cathodic hydrogen evolution overpotential on logarithm of coating thickness at RN coatings obtained form gas phase sulfidized nickel electrodes and cathodically deposited nickel sulfide coatings; electrolysis temperature: 120 °C.

4.5.2. RN coatings from electrodeposited nickel sulfide coatings. In Fig. 12 the dependence of overpotential on coating thickness is also shown for RN coatings obtained by cathodic reduction of electrodeposited nickel sulfide. The coating thickness varies from 120 to 700 μm. Compared to nickel sulfide coatings by gas phase sulfidation two differences are obvious: (i) electrodeposited coatings need to be approximately twice as thick as gas phase sulfidized coatings to obtain comparable overpotential reductions, and (ii) the correlation is somewhat steeper than for gas phase sulfidized coatings with $d\eta/d \log d$ equal to 70 mV decade^{-1} for 50 mA cm^{-2} and 95 mV decade^{-1} for 1 A cm^{-2}. Current potential curves become flatter the thicker the coating.

4.6. *Coulometric determination of the inner surface of RN catalysts*

Figure 13 shows the principle of coulometric surface determination. The RN coating is oxidized after cathodic polarization with a steady anodic current of ~2 mA cm^{-2}. At potentials below +100 mV vs RHE the hydrogen, adsorbed on nickel or dissolved in the pore electrolyte, is oxidized [40]. Between +100 mV and +300 mV there follows the nucleation of nickel hydroxide on the inner surface of the catalyst. This process lasts for RN coatings approximately 100 s. A further steady increase of the potential from 300 to approximately 1350 mV occurs in 350 to 450 s,

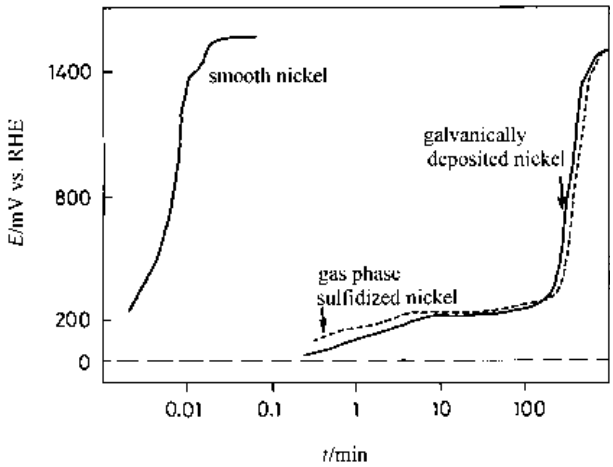

Fig. 13. Potential against $\log t$ plot for coulometric anodic oxidation of smooth nickel electrodes and RN coatings from cathodically deposited NiS_x (load: 51 mg cm^{-2}) and sulfidized (load 27 mg cm^{-2}) nickel (broken line).

respectively, and indicates the closure of the $Ni(OH)_2$ layer ending with the onset of the further oxidation of $Ni(OH)_2$ to NiOOH associated with a temporal halt of potential around 1350 mV. A fast final increase to the oxygen evolution potential of approximately 1500 mV signals completion of NiOOH formation. The galvanostatic oxidation is performed with current densities of 1.8, 1.7 and 1.6 mA cm^{-2} at smooth nickel and the two RN coatings, one obtained from cathodically deposited Ni_xS_y and the other from gas phase sulfidized nickel. 4.3×10^{-4}, 14 and 15 A s cm^{-2} are consumed for the reaction of Ni to NiO. The nominal nickel sulfide loadings amounted to 27 and 51 mg cm^{-2}. At perforated nickel foil with 41% open area nominal nickel sulfide loadings of 27 and 51 mg cm^{-2} correspond to true nickel sulfide loadings of 45 and 85 mg cm^{-2}. The nickel sulfide layers have a thickness of 83 and 157 μm. From this and the coulometric data the mass related surface of the catalyst is calculated to be 160 m^2 and 92 m^2 active surface per g of RN coating (basis is a specific current time integral of 5 A s m^2 of smooth nickel). These data are shown in Table 2 together with those obtained for a 75 μm RN coating from sherardized nickel [17]. Obviously RN from gas phase sulfidized nickel exhibits substantially more active surface than that obtained by galvanic NiS_x deposition or by sherardizing, which both almost match. Determining the surface of smooth, perforated nickel anodes coulometrically gives an effective surface ratio (related to the true, exposed surface of the electrode) of 1.3 cm^2 cm^{-2}, confirming the plausibility of the applied method.

5. Discussion

This investigation showed that nickel sulfide coatings quickly transform into RN coatings so that electrode kinetic investigations published on fresh NiS_x-coatings [41] seem to be of little practical relevance. The more recent investigations on particulate RN coatings on hydrogen evolving cathodes aim at determining rate coefficients according to the Tafel, Volmer and Heyrovsky scheme ([5–13, 42] and most recently [43], comparing NiS and NiZn coatings). The present authors refrain from this type of interpretation. The reason is the particular morphology of smooth RN coatings. These coatings form closed, homogeneous nanoporous layers with a thickness of 50 to 100 μm. The present authors have shown and recently discussed, [17, 44], that at low current densities only a relatively small fraction of the inner surface of smooth RN coatings is utilized because of concentration polarization by dissolved hydrogen. But these coatings become more and more utilized at higher current density and overpotential. Therefore, the analysis of the current voltage curves of such electrodes at low overpotential cannot serve for identifying the detailed electrode kinetics and determining rate coefficients. The authors have also shown that the small particles in composite RN coatings, which measure only a few micrometres in diameter, are fully utilized at low current densities, as far as they are not gas blanketed. Therefore the aforementioned kinetic approach may be applied to them. The investigations of Pschenichnikov *et al.* [42] on RN coatings obtained from smooth Ni/Al precursor coatings would be a more appropriate comparison to the present investigation. Pschenichnikov *et al.*'s data for high current densities confirm the decrease of overpotential with the logarithm of the

Table 2. Loadings and active inner surface of RN coatings obtained from two different NiS_x and a Ni/Zn precursor coating on perforated nickel sheet electrodes

	RN from gas phase sulfidized electrodes	*RN from cathodically deposited nickel sulfide*	*RN from sherardized nickel*
Deposited amount/mg cm^{-2}	9.6 (S)	51 (NiS_x)	48 (Zn)
Deposited 'NiY_x'/mg cm^{-2}	27 (Ni_7S_6)	51 (NiS_x)	60($Ni_{0.2}Zn_{0.8}$)
True* NiY_x loading/mg cm^{-2}	45 (Ni_7S_6)	85 (NiS_x)	100($Ni_{0.2}Zn_{0.8}$)
Thickness of coating/μm	83	157	75
True* loading of RN/mg cm^{-2}	29	54	20
Coulometric charge/A s cm^{-2}	14	15	6
True* charge/A s cm^{-2}	23.3	25	10
True inner RN surface/m^2 cm^2	4.66	5	2
Mass related inner surface/m^2 g^{-1} Ni	~160	~90	100

* true means accounting for 40% transparency of the perforated nickel sheet

coating thickness, in agreement with the present findings shown in Fig. 12, [17]. Although Pschenichnikov *et al*. were aware of the supersaturation of hydrogen in nanopores, as they observed the release of hydrogen at the rearside of the electrodes, they did not realize the consequence with respect to the limited degree of utilization of these coatings at low overpotential.

6. Conclusion

As smooth, closed RN coatings are shown to maintain low Tafel slopes even at current densities as high as $1\,A\,cm^{-2}$, they are at an advantage compared to composite RN coatings. Increasing their thickness helps to decrease the overpotential at high current densities. But since η decreases with the logarithm of the coating thickness, RN coatings thicker than $100\,\mu m$ are of little advantage. Above that thickness RN coatings become mechanically unstable and susceptible to thermal cycling. RN coatings from gas phase sulfidized nickel electrodes create the most stable and most effective electrocatalyst. Since operating gas phase reactions with dihydrogen sulfide on a technical scale is expensive and dangerous the easier sherardizing would be preferred and could be easily converted to industrial practice. It would be desirable to decrease the zinc content of the precursor coating from 80 to 65% for instance by limiting the amount of deposited zinc and to find a way to slow down the caustic leaching by at least one order of magnitude, for instance by leaching at low temperatures and using an alkaline aqueous methanol solution, in order to obtain a simultaneously more stable and more active smooth RN coatings.

References

[1] S. Trasatti, *in* Advances in Electrochemical Science and Technology', (edited by H. Gerischer and W. Tobias), vol. 2, VCH Weinheim (1990), p. 1.
[2] T. A. Liederbach, A. M. Greenberg and V: H: Thomas, *in* 'Modern Chloralkali Technology' (edited by M.O.Coulter), Ellis Horwood, Chichester (1980), p. 145.
[3] J. M. Müller, K. Lohrberg and H. Wüllenweber, *Chem. Ing. Techn.* **25** (1980) 435, *Germ. Offenleg. DE 2 829 901; Chem. Abs.* **92** (1980) 17162u; E. Endoh, H. Otouma, T. Morimoto, *Int. J*, *Hydrogen Energy*, **13** (1988) 207.
[4] H. Wendt and V. Plzak, *in* 'Electrochemical Hydrogen Technologies' (edited by H. Wendt), Elsevier Oxford (1990), pp. 15–62.
[5] L. Chen and A. Lasia, *J. Electrochem. Soc*. **139** (1992) 3214.
[6] Y. Choquette, L. Brossard, A. Lasia and H. Menard, *Electrochim. Acta*, **35** (1990) 1251.
[7] A. K. Cheong, A. Lasia and J. Lessard, *J. Electrochem. Soc*. **140** (1993) 2721.
[8] L. Chen and A. Lasia, *ibid* **138** (1991) 3321.
[9] A. Rami and A. Lasia, *J. Appl. Electrochem.* **22** (1992) 376.
[10] P. Los, A. Rami and A. Lasia, *ibid.* **23** (1993) 135.
[11] Y. Choquette, H. Menard and L. Brossard, *Int. J. Hydrogen Energy* **14** (1989) 637.
[12] L. Brossard, **13** (1988) 315.
[13] Y. Choquette, L. Brossard, A. Lasia and H. Menard, *J. Electrochem. Soc*. **137** (1990) 1723.
[14] Y. Choquette, L. Brossard and H. Menard, *J. Appl. Electrochem.* **20** (1990) 855.
[15] A. Kaiser, V. Borck, M. von Bradtke, R. Henne, W. A. Kaysser and G. Schiller, *Z. Metallkunde* **83** (1992) 7.
[16] Th. Borucinsky, S. Rausch and H. Wendt, *J. Appl. Electrochem.* **22** (1992) 1031.
[17] S. Rausch and H. Wendt, *J. Electrochem. Soc.* **143** (1996), 2852.
[18] B. Massalski, 'Binary Alloy Phase Diagrams', vol 1, American Society of Metals, Metals Park, OH (1986), p. 44073.
[19] A. J. Morton, *Acta Metallurgica* **27** (1979) 863.
[20] W. Vogelbier, B. P. Predat and Y. A. Chang, *Z. Metallkunde*, **73** (1982) 530.
[21] S. Budurov and B. Wassilev, *ibid.* **68** (1977) 795.
[22] L. G. Sillen, A. E. Martell, 'Stability Constants', The Chemical Society, Burlington House, London (1964); 'Stability Constants of Metal-Ion Complexes', Suppl. 1, The Chemical Society, Burlington House, London (1971).
[23] J. Bargel and G. Schulze, 'Werkstoffkunde', VDI-Verlag, Düsseldorf (1988).
[24] I. Barin, 'Thermochemical Data of Pure Substances', vols 1 and 2, VCH, Weinheim, (1989).
[25] R. E. F. Einerhand, W. H. M. Visscher and E. Barendrecht, *Electrochim. Acta* **34** (1989) 345.
[26] E. V. Proskupin and N. S. Gorbunov, 'Galvanizing, Sherardizing and Other Zinc Diffusion Coatings', Technology Ltd, Stonehouse, Gloucestershire, UK (1972).
[27] W. Heike, J. Schramm and O. Vaupel, 'Der Gefügebau von Nickel-Zinklegierungen in Metallwirtschaft, Metallwissenschaft, Metalltechnik', G.Lüttke, Hergb. Helm Verlag, Berlin, vol. **11** (1932), p. 539.
[28] H. Fischer and H. W. Dettner, *in* Ullmanns Enzyklopädie der Technischen Chemie' (edited by E. Bartholomé, E. Biekert, H. Hellmann, H. Ley, W. P. Weigert) part 4, vol. 12, VCH, Weinheim, (1976), p. 182.
[29] K. Widding, K. N. Andreasen and J. B. Holte, Norsk Hydro S/A, 'Active cathodes for electrochemical processes', *Ger. Offenl. DE 2 807 624*, 31 Aug. (1978).
[30] H. H. Ewe, E. W. Justi, A. W. Kalberlah and A. F. Schmitt, *Energy conversion* **12** (1972) 117.
[31] M. Bauer, H. H. Ewe and E. W. Justi, *ibid.* **12** (1972) 149.
[32] J. Freel, W. J. M. Pieters and R. B. Anderson, *J. Catal.* **14** (1969) 247.
[33] J. C. P. D. S. Powder Diffraction File, International Center for Diffraction Data, Swathmore, PA (1986).
[34] G. Tamm, *Z. Anorg. Allgem. Chem*. **111** (1920) 78.
[35] N. B. Pillings and R. E. Bedworth, *J. Inst. Metals* **29** (1923) 529.
[36] A. Dravnieks, *J. Electrochem. Soc.* **102** (1955) 252.
[37] F. Riccicerdiello and S. Roiotti, *Corros. Sci.* **12** (1972) 651.
[38] K. Hauffe and A. Rahmel, *Z. Phys. Chem*. **199** (1952) 152.
[39] R. A. Meussner and C. E. Birchenall, *Corrosion* **13** (1957) 677.
[40] A. G. Pschenichnikov, R. Ch. Burshtein and V. D. Kovalevskaya, *Elektrochymia* **11** (1975) 1465.
[41] H. Vandenborre, Ph. Vermeiren and R. Leysen, *Electrochim. Acta* **29** (1984) 297.
[42] A. G. Pschenichnikov, S. F. Cheruyshor, Yu. I. Kryokov, L. I. All'tentaller, E. I. Tumasova and V. N. Dudin, *Elektrochymia* **18** (1982) 1001.
[43] M. J. DeGiz, M. Fereira, G. Tremilosi-Filho and E. R. Gonzales, *J. Appl. Electrochem.* **23** (1993) 641.
[44] S. Rausch and H. Wendt, *ibid.* **22** (1992) 1025.